

Article

Evaluation of Anti-Skid Performance of Asphalt Mixture Based on Accelerated Loading Test

Houzhi Wang ¹, Yixuan Liu ¹, Jun Yang ^{1,*}, Xudong Shi ¹, Xinquan Xu ^{1,2}, Sang Luo ³ and Wei Huang ⁴¹ School of Transportation, Southeast University, Nanjing 211189, China² Guangdong Hualu Traffic Technology Co., Ltd., No. 1180 Guangcong Eighth Road, Guangzhou 510435, China³ Intelligent Transportation Systems Research Center, Southeast University, Nanjing 211189, China⁴ Nanjing Modern Comprehensive Transportation Laboratory, Nanjing 211189, China

* Correspondence: yangjun@seu.edu.cn

Abstract: Anti-skid performance is the most critical indicator that reflects the safety performance of the road surface. A good anti-skid performance of the road surface guarantees the safe and fast driving of vehicles. However, the asphalt pavement of highways has gradually exposed the anti-skid performance attenuation, which affects driving safety. Therefore, this study aims to accurately evaluate the anti-skid durability of asphalt mixtures based on a 1/3-size accelerated loading test with different anti-skid surfaces as the research object and explores the key factors affecting the long-term anti-skid performance of asphalt mixtures. The texture depth test and the pendulum value test show that the anti-skid durability of the SMA asphalt mixture is better than that of the AC asphalt mixture. The attenuation prediction equation of the British Pendulum Number (BPN), an anti-skid performance index based on an indoor accelerated loading test, was constructed. After the accelerated loading test stabilized, the BPN and BPN attenuation rate b were used as an index to evaluate the anti-skid durability of the asphalt mixture.

Keywords: accelerated loading; structural depth; pendulum value; performance evaluation



Citation: Wang, H.; Liu, Y.; Yang, J.; Shi, X.; Xu, X.; Luo, S.; Huang, W.

Evaluation of Anti-Skid Performance of Asphalt Mixture Based on Accelerated Loading Test. *Appl. Sci.* **2023**, *13*, 4796. <https://doi.org/10.3390/app13084796>

Academic Editors: Kezhen Yan, Jiaqi Chen and Jun Xie

Received: 27 February 2023

Revised: 3 April 2023

Accepted: 6 April 2023

Published: 11 April 2023



Copyright: © 2023 by the authors. Licensee MDPI, Basel, Switzerland. This article is an open access article distributed under the terms and conditions of the Creative Commons Attribution (CC BY) license (<https://creativecommons.org/licenses/by/4.0/>).

1. Introduction

Asphalt pavement, a composite material commonly used in road and bridge engineering, has been subjected to increasing traffic pressure and external environmental factors. This has resulted in a decline in the quality of aggregates used in road construction, impacting the macrotexture and microtexture of road surfaces and leading to the rapid deterioration of the anti-skid materials on the surface. The resultant weakening of the frictional force between tires and road surfaces can significantly reduce the performance of the road, posing a severe threat to the safety of people's lives and property. In this regard, the interrelationship between the friction of asphalt pavement and road safety is of paramount importance. Macrotexture, a pivotal contributor to frictional levels, plays a crucial role in ensuring road safety [1]. An accurate assessment of macrotexture at the inception of a pavement's life is critical. However, the skid resistance of newly constructed roads is highly variable due to the bitumen's masking effect on the aggregates. Therefore, it is crucial to build anti-skid surfaces using scientific and reasonable methods, study the anti-skid decay characteristics of pavement, and evaluate the anti-skid performance of asphalt pavement [2,3]. Although several scholars have developed indoor asphalt mixture accelerated abrasion equipment [4–15], there is currently no fully mature method for evaluating the anti-skid durability of asphalt mixtures.

The anti-skid performance of asphalt pavement is an essential factor in ensuring driving safety and comfort, and a key performance indicator for highway maintenance and construction. As such, it has garnered significant domestic and international attention from scholars. In one study, Chen [16] utilized a self-developed accelerated loading kneading

machine and pressure-sensitive technology to evaluate the skid-resistance decay characteristics of asphalt mixtures through a static pressure-sensitive film test on the asphalt pavement rutting plate. Rezaei [17] developed a model expressing skid resistance as a function of mixture gradation, aggregate texture, and traffic level based on comprehensive measurements and analysis of asphalt mixture surface characteristics in laboratory and field settings. Wang [18] investigated the stress distribution of static contact between tire and asphalt pavement under different roughness and kneading times for large-skid pavement using a pressure-sensitive film and an accelerated load kneading machine. Liu [19] analyzed the influence of mixture design parameters on the skid resistance of SMA pavement to obtain excellent skid resistance. Hofko [20] developed a prediction model for skid and polishing resistance based on the Wehner/Schulze device to predict the skid resistance level of a road surface after years of traffic. Ferkous [21] explored the skid resistance of asphalt concrete mixtures made of local low-performance aggregates by partially replacing sand with olive mill waste (OMW). Villani [22] discussed an innovative method to characterize the texture and friction of asphalt concrete mixes and their evolution over time. Xiong [23] investigated the anti-skid performance of an asphalt mixture composed of calcined bauxite and limestone aggregate, analyzing the pavement surface's friction variations based on the aggregates' differential polishing principle, and discussing the regularities of the distribution of the mean profile depth (MPD) of the asphalt pavement surface.

The small accelerated loading test is widely accepted as an effective method to evaluate the performance of asphalt pavements, given its capability to simulate actual traffic conditions indoors or on engineering sites and perform accelerated loading tests on full-scale pavements within a relatively short time using a controllable axle load. Consequently, it accurately assesses the long-term performance of the pavement structure or material under the negative impact of actual traffic loads over a prolonged period. It verifies the effectiveness of the pavement performance equation [5–9]. The present study employs a small accelerated loading test system, PAVEMLS11, to investigate asphalt mixtures' attenuation characteristics and anti-skid durability.

This study investigates the anti-skid durability of asphalt mixtures using a 1/3 size accelerated loading test and various anti-skid surfaces. Key factors that affect the long-term anti-skid performance of asphalt mixtures, including aggregate lithology, gradation, and oil-stone ratio, are explored. The novelty of this study lies in the systematic analysis of the effects of different aggregates, such as diabase, on the anti-skid resistance of the asphalt mixture. Skid resistance is evaluated through texture depth and pendulum value tests on six groups of AC and SMA asphalt mixtures. An anti-skid performance index, measured by the British Pendulum Number (BPN), is established based on laboratory accelerated loading tests. The BPN and its attenuation rate (B) after the stability of the accelerated loading test are used as the index of the anti-skid durability of the asphalt mixture.

The flowchart of the study is shown in Figure 1:

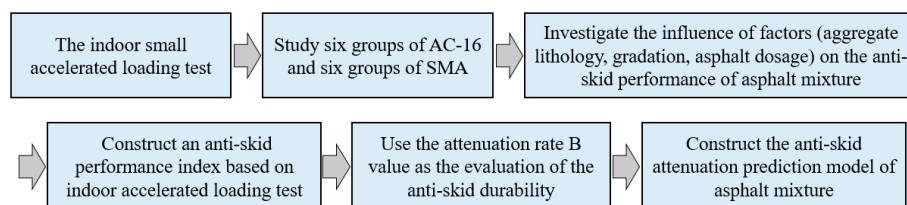


Figure 1. The flowchart.

2. Methods

2.1. Test Design

The present study employed a compact accelerated loading test system, PAVEMLS11, designed and manufactured by PaveTesting Ltd. (Letchworth Garden City, UK). As depicted in Figure 2, this system is a 1/3-scale model, notable for its compact size and ease of transport. It is highly suitable for indoor accelerated loading and field-testing research.

Further elaborating on the equipment, the system's configuration, and its technical specifications are explicated below.



Figure 2. Accelerated loading test equipment.

The equipment consists of a 1/3-size accelerated loading test system host, controller, wet heating system, test tank, dry heating/cooling system, laser profiler, indoor compression molding machine, etc. The equipment specifications include: ① Equipped with four test wheels, the effective test length is 1.1 m; ② Wheel load: 1.9~2.9 kN; ③ Pressure loading: 0.56 MPa~0.9 MPa; ④ Test wheel width of 80 mm and test width of 80~230 mm with lateral circulation function; ⑤ Test wheel speed: 0.5~2.5 m/s (1.8~9 km/h); ⑥ Maximum load repetitions: 7200 times/h; ⑦ The depth of the testable track is greater than 10 mm.

2.2. Materials

This study investigates the influence of internal factors, such as aggregate characteristics, gradation, and asphalt content, on the anti-skid surface layer's anti-skid performance. To explore the anti-skid durability of the anti-skid surface asphalt mixture, the research focuses on three anti-skid resistance types: AC-16, SMA-13, and SMA-10. The single-factor variable principle is adopted to examine the effect of oil-stone ratio, gradation, aggregate type, and other factors on the anti-skid durability of the asphalt mixture. The AC-16 asphalt mixture is prepared using three aggregates: andesite, diabase, lime, and SBS-modified asphalt (PG76-22). Six sets of asphalt mixture ruts with different oil-stone ratios, gradations, and lithologies are subjected to accelerated loading tests to assess the influence of various factors on the anti-skid durability of the AC-16 asphalt mixture. The SMA asphalt mixture is also examined by preparing five sets of SMA-13 slab specimens for rutting with different oil-stone ratios, gradations, and lithologies using two aggregates of andesite and diabase and SBS-modified asphalt (PG76-22). A set of SMA-10 slab specimens for rutting is also prepared as a comparison, and various factors' influence on SMA's anti-skid durability is studied. The specific test plan is presented in Table 1.

The technical indices of the three types of coarse aggregates utilized in this study are presented in Table 2, while Table 3 displays the test results for the fine aggregates. The gradation design outcomes of the asphalt mixture are illustrated in Figure 3.

Table 1. Experiment plan.

Test Number	Mixture Type	Gradation	Aggregate Type	Oil-Stone Ratio
S1	AC-16	Coarse	Diabase	4.4
S2	AC-16	Coarse	Diabase	4.9
S3	AC-16	Coarse	Diabase	5.4
S4	AC-16	Coarse	Diabase	4.9
S5	AC-16	Medium	Andesite	4.9
S6	AC-16	Coarse	Limestone	4.9
S7	SMA-13	Coarse	Diabase	5.8
S8	SMA-13	Medium	Diabase	6.0
S9	SMA-13	Medium	Diabase	6.2
S10	SMA-13	Coarse	Diabase	5.8
S11	SMA-13	Medium	Andesite	5.8
S12	SMA-10	Medium	Diabase	6.3

Table 2. Coarse aggregate technical index test results.

Test Index	Andesite	Diabase	Limestone
Crush value/%	9.4	13	20.4
Abrasion value/%	10.6	14.3	23.7
Polishing value/%	46	44	38

Table 3. Fine aggregate technical index test results.

Test Index	Test Results
Sand equivalent/%	68
Angularity/s	35.3

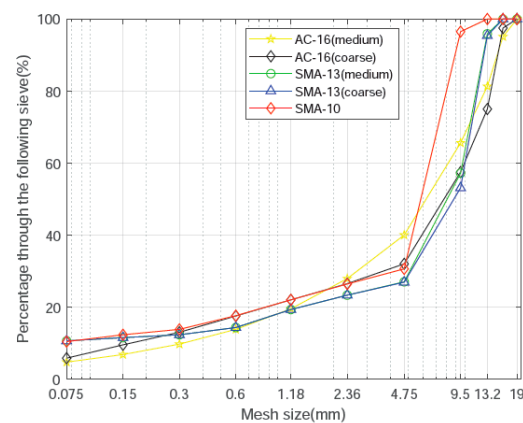


Figure 3. Asphalt mixture grading.

2.3. Experimental Procedures

The MLS11 accelerated loading test comprises a series of distinct steps, which include the formation of slab specimens for polishing, the processing of standard test pieces, the installation of said test pieces, the adjustment of equipment parameters, the actual loading test, and the subsequent collection of anti-skid data. The following sections delineate these steps in detail.

(1) Preparation of the test sample

In accordance with the T0703 test method specified in the “Highway Engineering Asphalt and Asphalt Mixture Test Regulations” (JTGE20-2011), the rut plate specimen for the asphalt mixture was prepared via the wheel rolling method, with dimensions of 300 mm × 300 mm × 50 mm. Subsequently, the rut plate was cut into test slabs of 150 mm × 150 mm × 50 mm using a cutting machine.

(2) Specimen installation

The standard test piece for asphalt mixture specified in the test plan should be installed in the test tank with utmost care. It should be noted that the height of the test piece may not be uniformly level during the installation process. To address this issue, the thickness of the steel plate beneath the test piece should be adjusted continuously until all three test pieces are aligned at the same level. Concurrently, the ends and nuts on both sides of the test mold must be tightened securely to prevent significant deviations of the test piece during the loading process.

(3) Loading test

① Load setting: In light of the most severe loading scenario, the maximum load of 2.7 kN is adopted for this test, and the wheel load calibrator is utilized to calibrate the load prior to testing. According to the stipulations, if the standard axle load is 100 kN for a single axle double wheelset and the load on a tire is 25 kN, the load for the accelerated loading test meets the requirements if it is reduced to 2.7 kN using a comparable constant of 1/9.

② Tire pressure: The test tire inflation pressure is 700 kPa.

③ Loading speed: The loading speed of the test adopts a maximum speed of 2.5 m/s (9 km/h), the frequency of the motor is 48 Hz, and the number of loads per hour is 7200.

④ Test temperature: The test is conducted under ambient temperature conditions, with a range of 20~25 °C. To maintain a consistent temperature for each test, the laboratory air conditioning temperature is set to 25 °C. The selected temperature range is representative of typical ambient temperatures that are suitable for both dry and wet states.

⑤ Dry and wet states: In order to simulate the humid conditions that are typical of hot and humid regions, water is added to the test tank during the accelerated loading test.

⑥ Number of loading times: The number of loading times varies from 0 to 600,000 cycles.

(4) Anti-skid and texture data collection

Subsequent to the completion of each loading sequence, the surface texture depth (MTD) and pendulum value of the asphalt mixture must be tested. Additionally, two-dimensional images of the asphalt mixture surface must be captured using a digital camera. To calculate the average section texture depth (MPD), data points along the two-dimensional structure line of the asphalt mixture surface must be obtained using the laser profiler integrated with the MLS11. A depiction of the data collection process is illustrated in Figure 4.

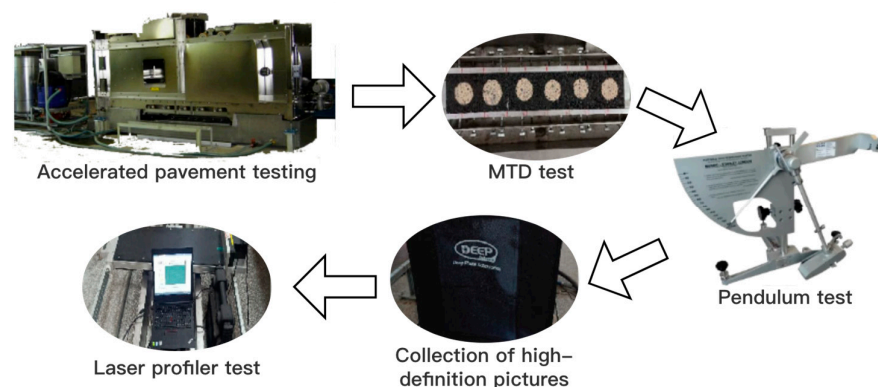


Figure 4. Data collection process.

To facilitate visual analysis of the anti-skid performance evaluation index attenuation amplitude for each mixture, an attenuation rate for the anti-skid performance has been defined, as described by Equation (1).

$$S = \frac{S_0 - S_{60}}{S_0} \times 100 \tag{1}$$

where:

- S is the attenuation rate of the anti-skid performance evaluation index (%);
- S₀ is the initial value of the evaluation index;
- S₆₀ is the final value of the evaluation index at the end of loading.

3. Result and Discussion

3.1. Texture Depth Test

The pavement texture depth, denoted as MTD, measures the macrotexture characteristics of road surfaces. Its magnitude positively correlates with the roughness of the road surface, which, in turn, aids in enhancing the drainage and safety of the pavement. Table 4 presents the MTD values before and after the application of 600,000 loading cycles, while Figure 5 illustrates the trend of MTD decay with increasing loading cycles.

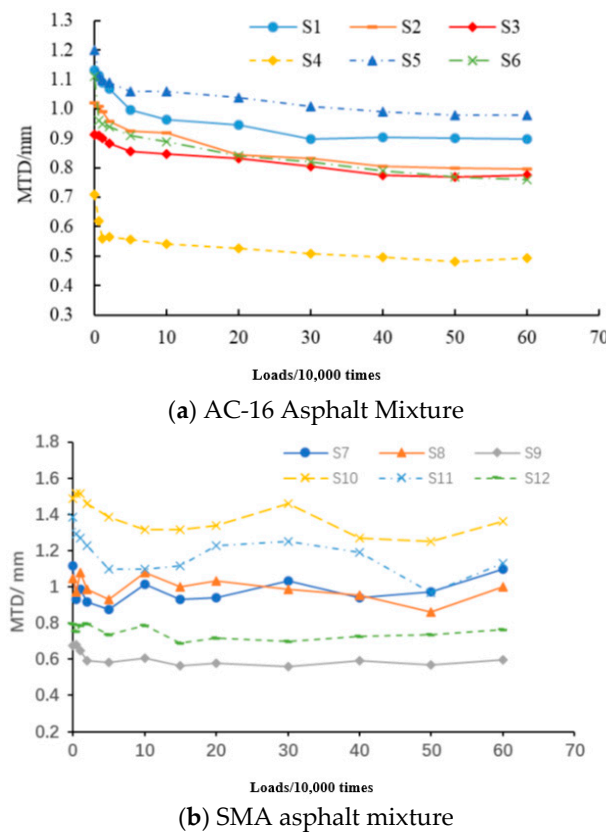


Figure 5. The relationship between MTD and accelerated loading times.

As depicted in Figures 5a and 6a and Table 4, it is widely acknowledged that the structural depth of compacted asphalt mixtures tends to increase with the greater content of coarse aggregate, a larger nominal maximum particle size, and a lower oil-stone ratio. The oil-stone ratios of S1, S2, and S3 are recorded at 4.4%, 4.9%, and 5.4%, respectively, thus resulting in the diminishing trend of macroscopic texture depth from S1 to S3. Additionally, S4’s 4.75 mm sieve pass rate increased from 32% to 40%, and the 9.5 mm sieve pass rate increased from 57.5% to 65.6%, along with the gradation becoming finer as compared to S2. Therefore, the initial MTD value of S4 is smaller than that of S2. Further, S5 and S6

are composed of andesites, while limestone has the same gradation. Consequently, the andesite asphalt mixture exhibits the highest initial MTD value compared to S2.

Table 4. Pavement structure depth and loading times.

Plan Number	MTD Initial Value/mm	MTD Final Value/mm	Attenuation Amplitude/mm	Attenuation Rate %	Mean Decay Rate/%
S1	1.13	0.90	0.23	20.60	20.60
S2	1.02	0.80	0.23	22.10	
S3	0.91	0.78	0.14	14.90	
S4	0.71	0.49	0.22	30.50	
S5	1.10	0.98	0.12	10.90	
S6	1.01	0.76	0.25	24.80	
S7	1.21	1.10	0.12	9.70	9.30
S8	1.05	1.00	0.05	4.50	
S9	0.67	0.60	0.08	11.30	
S10	1.49	1.36	0.13	8.60	
S11	1.38	1.13	0.25	18.00	
S12	0.80	0.77	0.03	3.90	

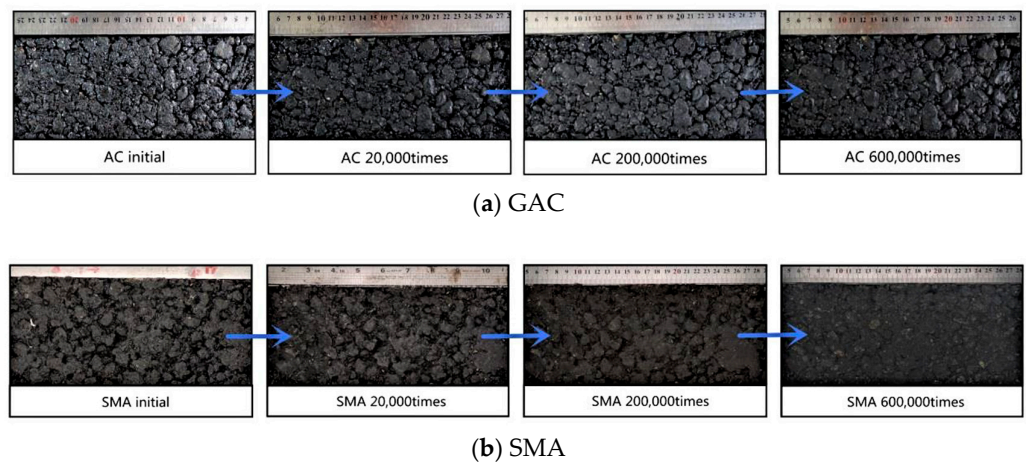


Figure 6. Surface changes of the asphalt mixture under different load repetitions.

The MTD values of the six AC-16 anti-skid surface layers exhibit a decreasing trend as the loading times increase. Specifically, a faster MTD decay rate is observed before loading 50,000 times, followed by a slowdown in the attenuation rate between 50,000 and 100,000 loading cycles. After 100,000 loading cycles, the MTD values of all programs remain stable. This phenomenon is mainly attributed to the slight compaction of the AC-16 asphalt mixture at the beginning of loading, leading to rapid MTD decay. However, as the loaded tire rubs against the asphalt mixture, the road surface particles become more compact, mitigating the impact of peaks and bumps on the road surface. The wheels' wear and tear also stabilizes road surface particles, resulting in a slower MTD decay rate.

Upon subjecting the six AC-16 anti-skid surface layers to 600,000 cycles of accelerated loading, the fine-graded S4 displayed the highest attenuation rate of MTD, followed by S6 (limestone aggregate). In contrast, S5 (andesite aggregate) exhibited the lowest MTD attenuation rate. This trend can be attributed to the relatively thin gradation used by S4, resulting in compaction deformation, rearrangement of road surface aggregates, and a substantial attenuation of MTD. The MTD value of S4 after 600,000 loading cycles was also the smallest among all programs. In contrast, S6 (limestone aggregate) displayed a relatively smooth aggregate surface, as evidenced by Figure 7c, and weak compaction ability between aggregates. This low compaction ability was linked to a low polishing value, a high abrasion value, and poor wear resistance.

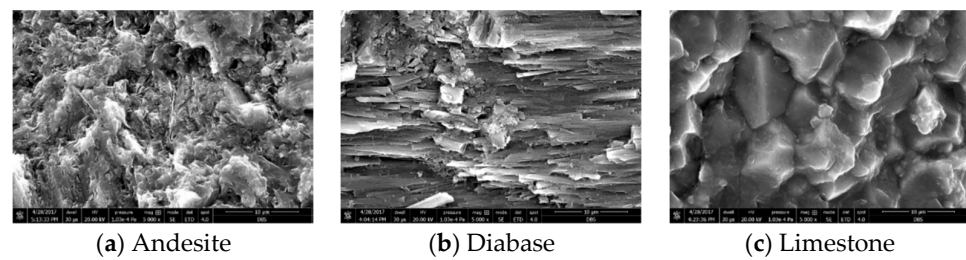


Figure 7. Scanning electron microscope photos of three kinds of aggregates (5000 \times).

Moreover, the rate of MTD decay of the anti-skid surface layer was determined by the polishing value and abrasion loss of the coarse aggregate under the same wheel load. The greater polishing value of the aggregate resulted in lower Los Angeles abrasion loss and a slower MTD decay rate of the anti-skid surface layer. Figure 7 presents scanning electron microscope photographs of three types of aggregates, with andesite and diabase aggregates exhibiting rough and angular surfaces with embedding solid capacities. In contrast, the surface of limestone was pomegranate-shaped, with relatively weak embedding capacity and inferior anti-skid performance compared to diabase and andesite aggregates.

The observations based on Figures 5b and 6b and Table 4 are presented as follows: The macrostructure depth of S7, S8, and S9 decreases with an increase in the oil-stone ratio. When the oil-stone ratio is the same, the pass rate of the 9.5 mm sieve in S10 is reduced from 57.2% to 53.1%, and the gradation becomes coarser, leading to a significantly larger initial value of the macrostructure depth for S4 than for S7. This demonstrates that for SMA-13, a coarser gradation leads to an increased macrostructure depth. S11, an SMA-13 mixture made of andesite aggregate, has a significantly greater initial texture depth than diabase aggregate-based mixtures with the same gradation. S12 is an SMA-10 mixture with a reduced nominal maximum particle size, resulting in a significantly decreased initial value of macrostructure depth compared to S7.

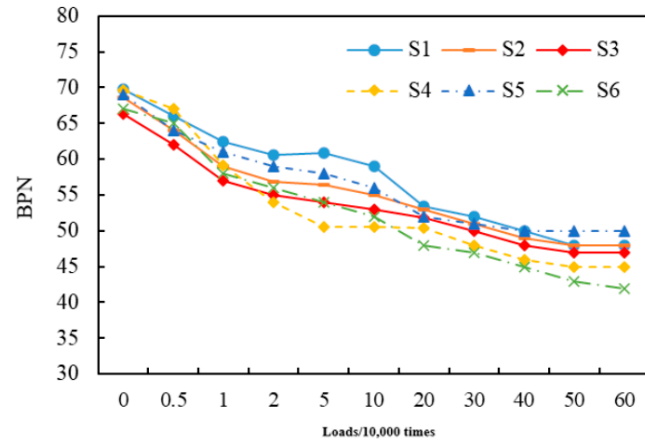
The observed structural behavior of six different SMA anti-skid surfaces under increasing loading cycles is investigated in this study. Contrary to the gradual reduction in MTD observed in AC-16, the structural depth of the six SMA anti-skid surfaces shows a wave-shaped variation with loading cycles, as depicted in Figure 5b. Specifically, the structural depth of S7, S8, S10, and S11 exhibits a decreasing trend before 50,000 to 100,000 loading cycles, followed by a slight upward trend. Subsequently, between 300,000 and 500,000 loading cycles, a decline in the structure depth is observed. This complex behavior is attributed to the relatively thick oil film in the SMA asphalt mixture that induces compaction during the initial loading stage, resulting in a decrease in the texture depth. However, with the action of the loaded tire and water erosion, the asphalt mortar between the surface of the SMA asphalt mixture and the aggregate gap will fall off, leading to an increase in the depth of its macroscopic structure.

Based on the results obtained after 600,000 loading cycles, the mean texture depth (MTD) attenuation rate was studied for various SMA anti-skid surfaces. S11, which utilized andesite aggregate, exhibited the highest attenuation rate of MTD, while S12 (SMA-10) had the smallest attenuation rate, followed by S8. This observation is attributed to the smaller nominal particle size and initial structural depth of S12, which resulted in a lower attenuation rate of its structural depth. For the SMA-13 anti-skid surface layer that employed diabase aggregate, S8 (oil-stone ratio of 6.0%) had the lowest attenuation rate of structural depth, followed by S10 (coarser gradation). These findings underscore the importance of employing a reasonable oil-stone ratio and coarser gradation to minimize the attenuation of macrostructure depth.

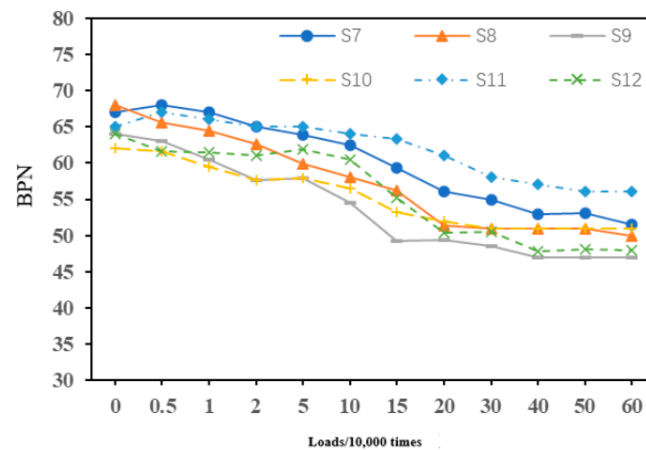
Following 600,000 load cycles, the mean attenuation rate for the macrostructure depth was determined to be 20.6% for the six groups of AC-16 and 9.3% for the six groups of SMA. The results suggest that the SMA asphalt mixture performed better than the AC asphalt mixture, as indicated by the attenuation rate index.

3.2. Pendulum Test

A road surface’s pendulum value indicates its microstructure; greater pendulum values correspond to a richer microstructure and a higher pendulum friction coefficient, indicating better anti-skid performance. Figure 8 demonstrates the trend in pendulum value attenuation with increasing loading times. Table 5 shows the initial pendulum friction coefficient value for each experimental scheme and the value after 600,000 loading cycles.



(a) AC-16 Asphalt Mixture



(b) SMA asphalt mixture

Figure 8. The relationship between BPN and accelerated loading times.

Table 5. Friction coefficient of pendulum and load repetitions.

Plan Number	Initial Value/BPN	Final Value/BPN	Attenuation Amplitude/BPN	Attenuation Rate %	Mean Decay Rate/%
S1	70	48	22	31.4	32.1
S2	69	48	21	30.4	
S3	66	47	19	28.8	
S4	70	45	25	35.7	
S5	69	49	20	29.0	
S6	67	42	25	37.3	
S7	67	52	15	22.4	22.3
S8	68	50	18	26.5	
S9	64	46	18	28.1	
S10	62	51	11	17.7	
S11	65	56	9	13.8	
S12	64	48	16	25.0	

The microstructure of a road surface can be characterized by its pendulum value, which is positively correlated with the pendulum friction coefficient and thus indicates better anti-skid performance. Figure 8a reveals that S1 and S4 have the largest initial pendulum values among the tested schemes. While the gradation curves of S1, S2, S3, S5, and S6 are similar, the gradation of S4 is finer. As the test pieces were prepared using the same molding method, differences in pendulum value can be attributed to independent factors such as the rolling process. S1 has a lower oil-stone ratio than S2, resulting in a higher initial pendulum value.

Conversely, an increased oil-stone ratio in S3 reduced the initial pendulum value. The thinner gradation of S4 increased its initial pendulum value, which could be related to a thinner oil film resulting from gradation thinning. S5 and S6 are andesite and limestone aggregates, respectively. They exhibited no significant difference in the initial pendulum value compared to S2, suggesting that aggregate lithology has a minimal impact on the initial pendulum value.

As the number of accelerated loading times increased, the pendulum values of the six anti-skid surface layers of AC-16 gradually decreased. A rapid decay state is observed in the pendulum values before loading 5000 times, which is attributed to the initial rapid wear of the spikes and bumps of the road surface by the loading wheel, leading to faster decay of the friction coefficient BPN. From 10,000 to 400,000 loading times, the pendulum value of each AC-16 scheme stabilized during attenuation. This is due to the wear of the bumps and spikes of the anti-skid road surface, which stabilizes the anti-skid performance of the road surface, which is mainly determined by the micro-texture of the aggregate. The friction coefficient of the road surface remains stable. After being loaded 400,000 times, the friction coefficient of AC-16 is stable as the texture of the road surface is worn to a certain extent and the macro and microtextures of the road surface reach a stable state.

Upon conducting the 600,000-time loading test, it was observed that the final pendulum values of S1, S2, and S3 are relatively consistent, implying that the oil-stone ratio's impact on the pendulum value is negligible. The fine gradation of S4, as compared to S2, results in a smaller final pendulum value. The andesite aggregate in S5 yields the highest final pendulum value among all schemes, while the limestone aggregate in S6 yields the lowest. Previous research indicates that the mechanical properties of coarse aggregate (i.e., polishing value, crushing value, and abrasion value) play a decisive role in the durability of asphalt pavement's anti-skid properties. Comparatively, the coarse aggregate used in S5 exhibits a slightly larger polishing value, smaller crushing value, and abrasion value than S3 and a greater pendulum friction coefficient after stabilization than S2. On the other hand, the pendulum friction coefficient of S6 after stabilization is less than that of S2, which can be attributed to the limestone aggregate's low wear resistance and angularity compared to the diabase aggregate in S2. Hence, this study validates that aggregate properties significantly influence the AC-16 asphalt mixture's anti-skid durability.

Figure 8b presents the analysis of the impact of the oil-stone ratio and aggregate gradation on the initial pendulum value of six AC-16 schemes, namely S7, S8, S9, S10, S11, and S12. Schemes S7, S8, and S9 have identical gradation curves but different oil-stone ratios. An increase in the oil-stone ratio is found to be associated with a decrease in the initial pendulum value. Scheme S10 has a relatively thicker gradation compared to S7, leading to a decrease in the initial pendulum value. This finding suggests that a thicker gradation is linked with a smaller initial friction coefficient under the same oil-stone ratio. Scheme S11 has the same gradation as S7 but uses coarse andesite aggregate. There is no significant difference in the initial pendulum value between the two, indicating that the lithology of the aggregate has a negligible effect on the initial pendulum value of the AC-type asphalt mixture. Scheme S12, an SMA-10, has a smaller nominal maximum particle size compared to S7 and a larger oil-stone ratio. As a result, the initial pendulum value of S12 is lower than that of S7.

As the loading test progressed, the pendulum values of the six SMA anti-skid surface layers gradually decreased, but the attenuation trend was not the same as that of AC-16.

In the initial loading stage (before 5000 times), S7 and S11 exhibited an increasing trend in the pendulum value, followed by a decay. This phenomenon can be attributed to the fact that, in the beginning, the texture of the road surface was covered by an asphalt film, resulting in a lower initial pendulum value. As the tires move and water washes over the road surface, the asphalt film partially peels off, exposing the aggregate texture that starts to resist skidding. Generally, the pendulum value of each scheme oscillated in a wave-like pattern between 10,000 and 400,000 loadings. This behavior can be linked to the asphalt film on the road surface wearing off after a certain number of loadings and the continuously wearing bumps and peaks on the road surface. During this time, the anti-skid performance of the road surface is determined by the micro-texture of the aggregate. The friction coefficient of the road surface is in a stable state. The road surface of SMA is relatively rough, which can affect the pendulum value test and result in a wave-like decline in the pendulum value. After 400,000 loadings, the friction coefficient of SMA stabilizes. This phenomenon can be attributed to the fact that after the road surface texture is worn to a certain extent, both the macro and microtextures stabilize.

Upon completion of a 600,000-time loading test, S11, which utilized andesite aggregate, exhibited the highest pendulum value after stabilization. This can be attributed to the superior mechanical properties of its coarse aggregate, as evidenced by its polishing value, crushing value, and abrasion value. Following the stabilization of AC-16, the pendulum value law of S11 is consistent with that of the former. On the other hand, S7, S8, and S9 comprised SMA-13 with varying oil-stone ratios. As the oil-stone ratio increases, the stable pendulum value decreases, a trend that is not in line with the stable pendulum value of AC-16. This indicates that the oil-stone ratio significantly impacts the stable value of the pendulum of the SMA-13. Compared to S7, the gradation of S10 is thicker, with a stable pendulum value similar to that of S7 after stabilization.

Furthermore, the pendulum value of S12 (SMA-10) after stabilization is slightly smaller compared to that of S7 (SMA-13). This is consistent with the principle that larger nominal particle sizes produce better anti-skid durability. Regarding the pendulum value attenuation rate index, S11 exhibits the lowest rate of attenuation, which can be attributed to the high polishing value, low crushing value, and high abrasion value of the aggregate used.

In summary, the results demonstrate that after 600,000 loadings, the average pendulum attenuation rates for the six groups of AC-16 and the six groups of SMA were 31.8% and 22.1%, respectively. This indicates that the SMA asphalt mixture exhibits superior anti-skid durability compared to the AC asphalt mixture.

3.3. Anti-Skid Performance and Durability Evaluation

3.3.1. Anti-Skid Attenuation Equation

At present, logarithmic and exponential equations are predominantly employed by both domestic and foreign researchers to anticipate the attenuation condition of anti-skid properties in asphalt mixtures [24]. The utilization of exponential and logarithmic equations to signify the attenuation pattern of the anti-skid index for asphalt pavements is denoted by Equations (2) and (3), respectively.

$$y = a_0 e^{-b_0 n} + c \quad (2)$$

$$y = a_1 - b_1 \log(n) \quad (3)$$

where:

y is the anti-skid index of the asphalt surface.

n is the number of axle loads (times).

a_0 , b_0 , c , a_1 , and b_1 are equation parameters.

To assess the suitability of Equations (2) and (3) for anti-skid surface layers in both AC and SMA, a comparison of anti-skid index BPN and MTD values of asphalt mixtures gathered during accelerated loading conditions was conducted utilizing the least squares principle. Nonlinear fitting was then utilized to examine the correlation between loading

times and the anti-skid index of the asphalt surface, and the equation parameters are presented in Tables 6 and 7. The results in Table 6 indicate that the correlation coefficient R^2 for the exponential equation and the logarithmic equation in MTD attenuation estimation are virtually identical. Furthermore, the prediction accuracy for the structural depth attenuation trend is relatively high. However, the effectiveness of predicting the structural depth attenuation trend in the SMA mixture is suboptimal, with the minimum value of the correlation coefficient R^2 at only 0.24. This outcome is primarily due to wave-like changes in the structural depth of the SMA mixture with an increasing number of loads, resulting in the equations' failure to deliver better outcomes.

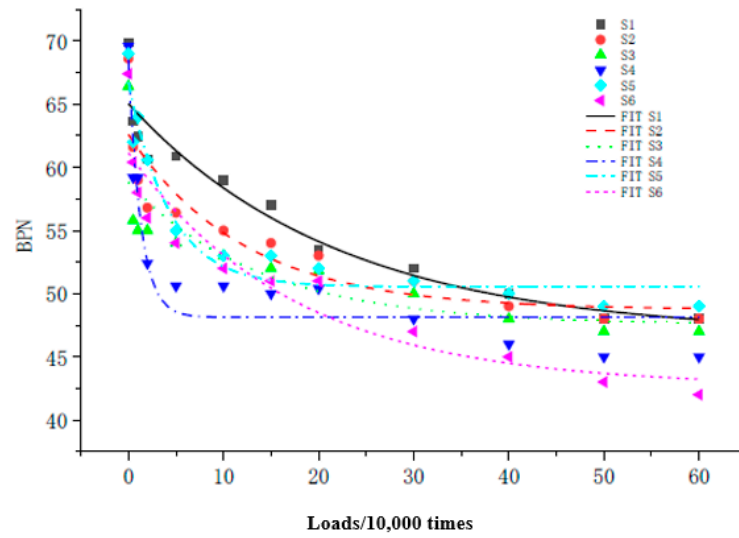
Table 6. MTD attenuation prediction equation parameters.

Plan Number	Exponential Equation						Adjusted R^2
	c		a_0		b_0		
	Value	Standard Error	Value	Standard Error	Value	Standard Error	
S1	0.91	0.01	0.22	0.01	-0.13	0.02	0.98
S2	0.79	0.01	0.21	0.01	-0.07	0.01	0.97
S3	0.76	0.01	0.14	0.01	-0.05	0.01	0.96
S4	0.52	0.01	0.19	0.03	-1.17	0.36	0.84
S5	0.98	0.02	0.15	0.02	-0.07	0.03	0.8
S6	0.77	0.03	0.23	0.03	-0.07	0.03	0.81
S7	0.93	0.00	0.28	0.00	-0.59	0.02	1
S8	0.97	0.02	0.19	0.05	-0.79	0.51	0.56
S9	0.58	0.01	0.11	0.02	-0.59	0.24	0.8
S10	1.31	0.02	0.21	0.03	-0.20	0.09	0.82
S11	1.15	0.02	0.23	0.06	-0.71	0.43	0.61
S12	0.73	0.01	0.06	0.02	-0.16	0.18	0.34
Plan Number	Logarithmic Equation						Adjusted R^2
	a_1		b_1				
	Value	Standard Error	Value	Standard Error			
S1	1.085	0.006	0.049	0.002			0.98
S2	0.992	0.008	0.046	0.003			0.96
S3	0.903	0.007	0.030	0.003			0.93
S4	0.587	0.007	0.023	0.003			0.89
S5	1.105	0.008	0.028	0.003			0.91
S6	0.959	0.011	0.043	0.004			0.92
S7	1.062	0.016	0.040	0.006			0.81
S8	1.061	0.026	0.031	0.100			0.48
S9	0.637	0.013	0.018	0.005			0.56
S10	1.493	0.019	0.061	0.007			0.89
S11	1.240	0.036	0.027	0.013			0.24
S12	0.775	0.015	0.017	0.005			0.46

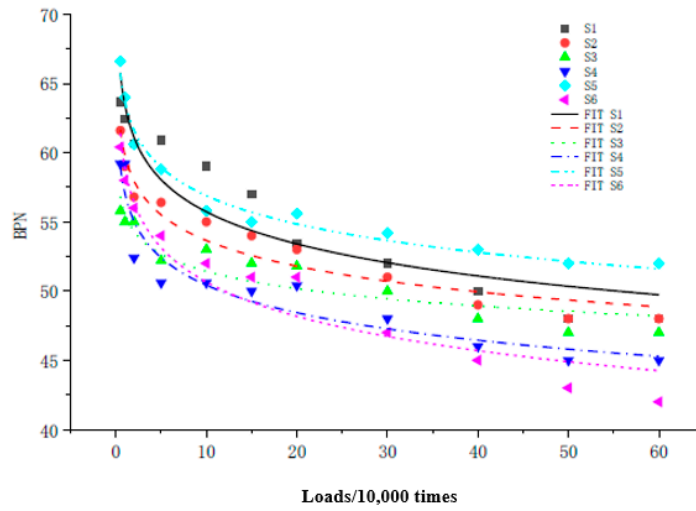
Table 7. BPN attenuation prediction equation parameters.

Exponential Equation								
Plan Number	c		a ₀		b ₀		Statistics	
	Value	Standard Error	Value	Standard Error	Value	Standard Error	Residual Sum of Squares	Adjusted R ²
S1	46.7	2.6	18.3	2.47	0.05	0.02	4.22	0.91
S2	48.7	1.8	13.9	2.1	0.08	0.04	7.27	0.8
S3	50.4	0.9	15.1	2.7	0.07	0.52	6.98	0.75
S4	48.1	0.9	20.4	2.4	0.77	0.22	6.08	0.88
S5	53.6	0.6	14.2	1.1	0.24	0.06	19.94	0.94
S6	42.6	2.6	18.5	2.63	0.06	0.02	7.87	0.86
S7	51.3	1.5	18.3	1.56	0.06	0.01	2.78	0.95
S8	49.6	1.1	16.8	1.28	0.07	0.02	2.48	0.95
S9	46.2	0.8	16.2	0.98	0.08	0.02	1.59	0.96
S10	49.6	0.7	11.6	0.9	0.1	0	1.2	0.9
S11	47.3	10.6	20	10.31	0.02	0.01	2.69	0.89
S12	45.6	2.5	17.9	2.33	0.04	0.01	3.07	0.93
Logarithmic Equation								
Plan Number	a ₁		b ₁		Residual Sum of Squares	Statistics		
	Value	Standard Error	Value	Standard Error		Adjusted R ²		
S1	64.2	1.03	3.60	0.38	3.82	0.90		
S2	60.6	0.68	2.94	0.25	1.64	0.94		
S3	58.4	0.62	2.69	0.23	1.39	0.93		
S4	60.0	1.20	3.81	0.44	5.19	0.88		
S5	61.6	0.41	3.00	0.15	0.61	0.98		
S6	60.6	0.86	4.27	0.31	2.64	0.95		
S7	67.3	0.77	3.60	0.28	2.22	0.94		
S8	64.3	0.64	3.51	0.24	1.49	0.96		
S9	61.1	0.42	3.24	0.15	0.63	0.98		
S10	61.4	0.80	2.81	0.29	2.32	0.90		
S11	66.4	1.83	2.27	0.31	2.50	0.84		
S12	63.3	1.00	3.56	0.36	3.56	0.90		

Table 7 reveals that the correlation coefficient R² for BPN attenuation estimation is essentially the same for the exponential equation and the logarithmic equation. However, the two equations emphasize the decay trend of asphalt mixture BPN in their respective ways. The fitting curve of the logarithmic equation has a better correlation coefficient, R², compared to the exponential equation. Additionally, the c value in the exponential equation represents the final attenuation value, and thus, it can only estimate the anti-skid index within the maximum load repetitions of 600,000 times. As a result, this study utilizes the logarithmic equation to anticipate the friction coefficient’s attenuation trend and evaluate the anti-skid durability of asphalt mixtures. The fitting curve diagrams of BPN and loading times, represented in Figures 9 and 10, illustrate that after a certain number of load repetitions, the BPN of the anti-skid surface layer exhibits a stable attenuation trend, which is consistent with the actual asphalt pavement’s lateral force coefficient attenuation trend. Figure 11 represents the comparison of BPN attenuation stability value and attenuation rate.



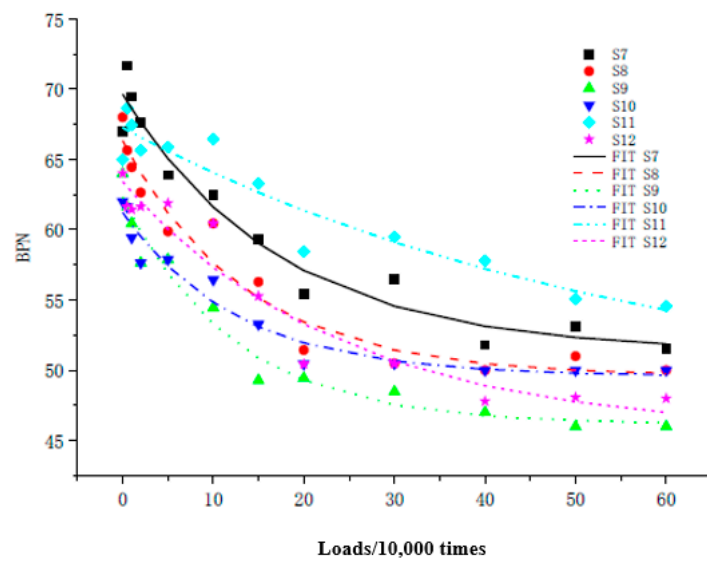
(a) Exponential equation fitting



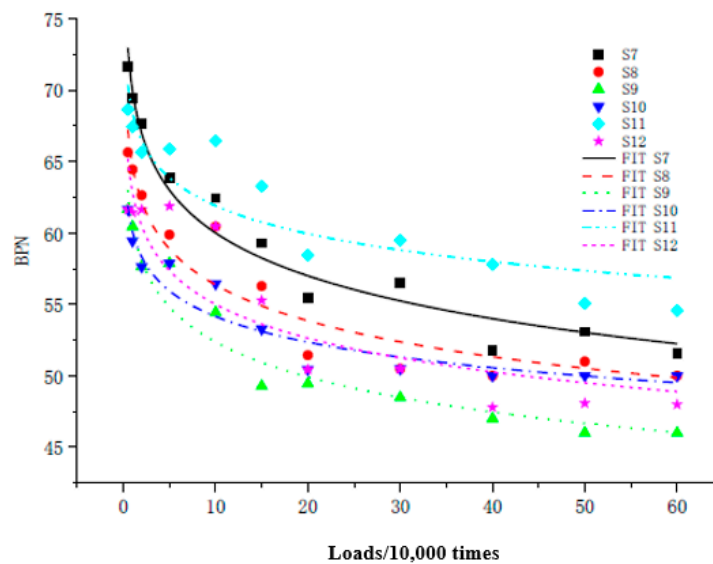
(b) Logarithmic equation fitting

Figure 9. Pendulum friction coefficient attenuation fitting curve (AC-16).

The anti-skid surface layer made up of various materials exhibits distinct pendulum friction coefficient attenuation rates, while the pendulum friction coefficient that reaches stability differs. The logarithmic equation's A value ($Y = A - B \times \ln(n)$) signifies the anti-skid index's initial value, which can typically be replaced by the anti-skid index value during the initial loading stage. The comparative analysis of the test outcomes demonstrates that the A value is quite close to the BPN during the initial loading stage (0.5 million times) with a relative error of less than 8%. Consequently, the BPN at the initial loading stage (0.5 million times) can substitute for the A value of the exponential equation. The B value reflects the decay rate of the anti-skid index, with a higher value indicating faster anti-skid index decay. Figure 12 illustrates a comparison diagram of the BPN decay rate (B value). For the AC-16 asphalt mixture, a greater oil-stone ratio corresponds to a lower pendulum decay rate. S6 (limestone) has the highest pendulum decay rate, while the diabase asphalt mixture's decay rate is intermediate, and the andesite asphalt mixture's decay rate is the lowest. The SMA asphalt mixture's ($B = 3.16$) pendulum decay rate is superior to that of AC-16 ($B = 3.39$). Hence, the logarithmic equation's B value can reflect the impact of diverse lithological aggregates, oil-stone ratios, gradations, etc., on the anti-skid durability of asphalt mixtures.



(a) Exponential equation fitting



(b) Logarithmic equation fitting

Figure 10. Pendulum friction coefficient attenuation fitting curve (SMA).

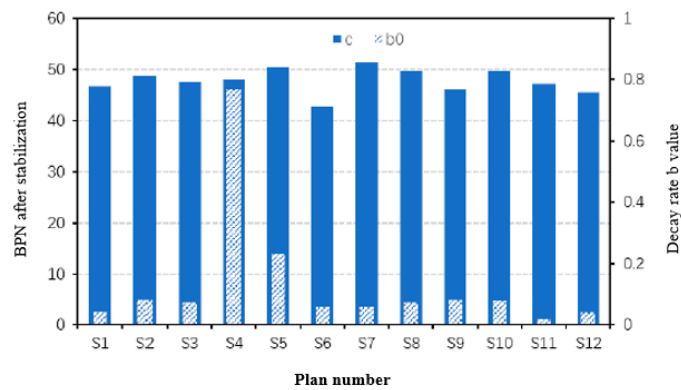


Figure 11. Comparison of BPN attenuation stability value and attenuation rate.

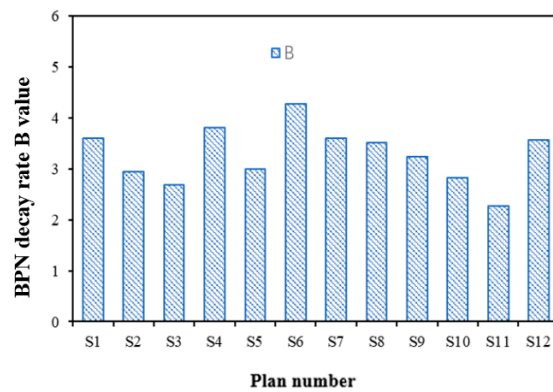


Figure 12. BPN attenuation rate comparison.

To investigate the effects of physical indicators of coarse aggregates, gradation, oil-stone ratio, and other parameters on the attenuation rate B value, statistical data of coarse aggregate properties, such as crushing value CSV, abrasion value WSV, polishing value PSV, P_{ai}/P_a (the actual oil-stone ratio to the best oil-stone ratio), as well as gradation scale factor λ and shape factor k , were collected and are presented in Table 8. Based on the analysis, it was found that the oil-stone ratio has a significant impact on the B value. For asphalt mixtures with the same gradation and coarse aggregate, a larger oil-stone ratio leads to a lower pendulum value attenuation rate, while a thicker gradation results in a lower pendulum value attenuation rate at the same oil-stone ratio. Moreover, the physical properties of coarse aggregates have a substantial impact on the B value. Therefore, the value of B depends on the asphalt mixture’s gradation, oil-stone ratio, and coarse aggregate mechanical properties (WSV and PSV). The relationship between the value of B and each key parameter can be described by Equation (4), which is constructed based on experimental experience, and the parameter values will be obtained through subsequent regression analysis.

$$B = B_1 \cdot WSV + B_2 \cdot PSV + B_3 \cdot \lambda + B_4 \cdot k + \frac{B_5 P_a}{P_{ai}} + C \tag{4}$$

Table 8. Index values of various parameters of the asphalt mixture.

Wear Value (WSV)	Polishing Value (PSV)	Size Factor λ	Shape Factor k	P_{ai}/P_a	B Value
14.3	44	8.332	0.944	0.9	3.6
14.3	44	8.332	0.944	1	2.94
14.3	44	8.332	0.944	1.1	2.69
14.3	44	7.469	0.972	1	3.81
10.6	46	8.332	0.944	1	3
23.7	38	8.332	0.944	1	4.27
14.3	44	8.253	1.266	1	3.6
14.3	44	8.253	1.266	1.03	3.51
14.3	44	8.253	1.266	1.07	3.24
14.3	44	8.494	1.262	1	2.81
10.6	46	8.253	1.266	1	2.27
14.3	44	6.054	1.266	1	3.56

After conducting regression analysis on the data from Table 8 using Equation (4), the index values of each parameter were obtained and are presented in Table 9.

Table 9. Regression analysis results for various parameters.

B₁	B₂	B₃	B₄	B₅	B₆	B₇
0.194	0.117	−0.236	−0.101	−3.136	0.500	0.986

By using the estimated expression (5) of the attenuation rate B, the pendulum decay rate of each scheme was calculated. As shown in Equation (5), a larger wear value of the coarse aggregate leads to a greater pendulum decay rate, while thicker gradation results in a lower pendulum decay rate. The calculated values of the attenuation rate B were then compared to the regression values obtained from the accelerated loading test data; the results are summarized in Table 10. The relative error between the calculated and regression values is small, with a maximum value of 12.1%. The B meter can replace the B value, and by incorporating Equation (5) into Equation (3), the prediction equation of asphalt mixture BPN attenuation, as shown in Equation (4), can be obtained.

$$B = 0.194 \cdot WSV + 0.117 \cdot PSV - 0.236 \cdot \lambda + 0.101 \cdot k + 3.136 P_a / P_{ai} + 0.5 \quad (5)$$

$$BPN = A - (0.194 \cdot WSV + 0.117 \cdot PSV - 0.236 \cdot \lambda + 0.101 \cdot k + 3.136 P_a / P_{ai} + 0.5) \ln(n) \quad (6)$$

Table 10. Attenuation rate B value comparison.

Number	B Value	Predicted B Value	Relative Error
S1	3.6	3.55	1.6
S2	2.94	3.23	−9.8
S3	2.69	2.91	−8
S4	3.81	3.43	10.2
S5	3	2.74	8.5
S6	4.27	4.35	−1.7
S7	3.6	3.21	10.7
S8	3.51	3.1	11.5
S9	3.24	3	7.7
S10	2.81	3.16	−12.1
S11	2.27	2.43	−7.2
S12	3.56	3.73	−4.9

Equation (6) represents the prediction model for the anti-skid performance of asphalt pavement under accelerated loading tests, where n denotes the number of acceleration loads and the cumulative axle number on the actual road surface is the total number of axle loads on the designed lane within a certain time period. However, since the number of axle loads on the wheel tracks follows a probability distribution, it is not possible to equate the cumulative load repetitions obtained from PAVEMLS11 with the actual cumulative axle load repetitions on the road surface. Therefore, to make Equation (6) applicable for predicting the anti-skid performance of actual asphalt pavement, it is necessary to establish a correlation between the cumulative number of indoor loads and the cumulative number of axle loads on the road surface, as shown in Equation (7).

Where: *n* is the cumulative loading times of PAVEMLS11, ten thousand times; *N_e* is the cumulative number of axle loads on the road surface, ten thousand times per lane; and *φ* is the lateral distribution coefficient of wheel tracks, %.

The lateral distribution coefficient of the wheel track refers to the proportion of times the vehicle undergoes a particular width, such as the width of the wheel track on the

cross-section of the lane. In the case of expressways, the lateral distribution frequency curve of the wheel track exhibits a hump-shaped distribution, as demonstrated in Figure 13.

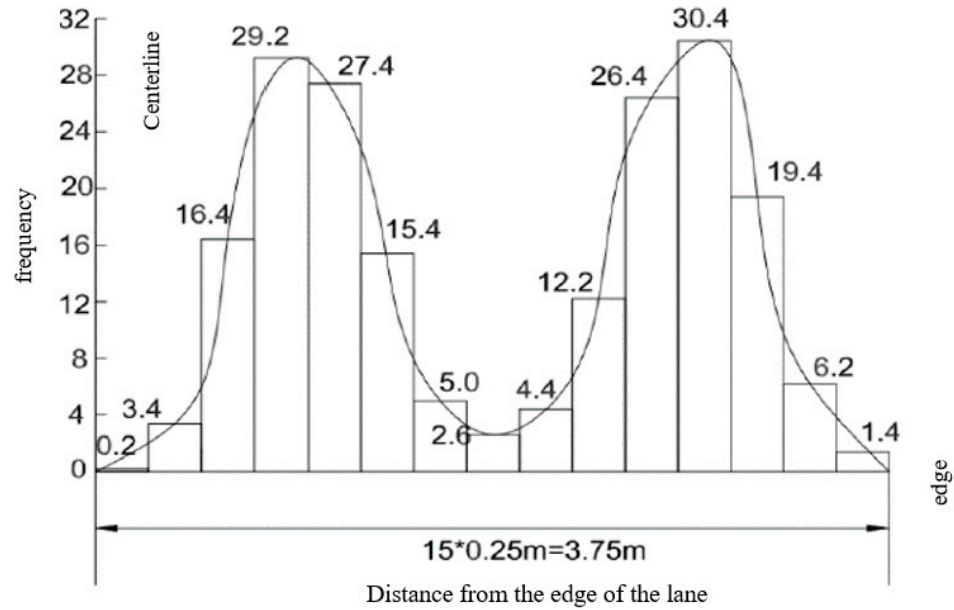


Figure 13. Wheel track transverse frequency distribution curve.

The findings presented in Figure 13 indicate that the peak frequencies of wheel loads occur at the 4th and 12th units from the edge of the lane, which correspond to the midpoint of the wheel track belt on the road surface. This region is subjected to the most wear and abrasion and is the primary test position for the pavement lateral force coefficient. Consequently, we have identified the 30.4% and 29.2% lateral distribution frequency points as the locations where the anti-skid performance deteriorates the most. Based on this information, we propose to define the lateral distribution coefficient of wheel tracks as follows:

$$\varphi = \frac{(30.4\% + 29.2\%)}{2} = 29.8\% \tag{7}$$

By means of the preceding analyses and computations, we have derived Equation (8), which characterizes the conversion correlation between the cumulative load repetitions (n) of PAVEMLS11 and the actual cumulative axle load repetitions (Ne) on the road surface.

$$n = 0.298N_e \tag{8}$$

Based on the measured SFC and BPN values and the correlation analysis results presented in this article, it is evident that BPN and SFC exhibit a strong linear correlation. A linear regression analysis was performed to establish the equation between SFC and BPN, which is depicted in Equation (9), and the correlation coefficient R was found to be 0.94, indicating a strong correlation between these two parameters.

$$SFC = 1.07 \times BPN - 4.6 \tag{9}$$

Accordingly, the substitution of Equations (6) and (8) into Equation (9) leads to the derivation of the prediction equation for actual asphalt pavement SFC, as presented in Equation (10). Both Equations (10) and (11) are the outcomes of regression analyses.

$$SFC = 1.07 \cdot (A - (0.194 \cdot WSV + 0.117 \cdot PSV - 0.236 \cdot \lambda + 0.101 \cdot k + 3.136 P_a / P_{ai} + 0.5) \ln(0.298 N_e)) - 4.6 \tag{10}$$

$$SFC = 10 - 3.085 \times \ln(CNAT) + 1.650 \times PSV + 0.730 \times \lambda + 6.552 \times k \tag{11}$$

The presented equation includes various factors relevant to predicting the lateral force coefficient of asphalt pavement, denoted as *SFC*. These factors include *A*, representing the initial value of the pendulum value of indoor slab specimens for rutting test blocks; *WSV*, referring to the loss rate of the coarse aggregate Los Angeles abrasion, expressed as a percentage; *PSV*, indicating the coarse aggregate polishing value; λ , the graded scale factor; *k*, the gradation form factor; and *N_e*, the cumulative number of axle loads of trucks, measured in ten thousand repetitions.

3.3.2. Equation Comparison

To assess the precision and dependability of the anti-skid performance attenuation equation (Equation (10)) of asphalt pavement obtained from the indoor accelerated loading test, the predictive equation was evaluated against test road observation data and compared with the on-site prediction equation (Equation (11)) in Tables 11 and 12. The results reveal that the *SFC* predicted values obtained from Equation (10) are marginally greater than the actual measured values, with a maximum relative deviation rate of 15.4%, and the predicted values of Equation (10) tend to be overestimated. The phenomenon is thought to be related to the lower ground pressure of the acceleration load test tire (0.7 MPa) than the actual truck tire ground pressure on the road. The minimum deviation rate in the five test sections is 3.7%, while the maximum deviation rate is 18.9%, with the absolute deviation of the predicted *SFC* varying between 2 and 12, indicating the prediction accuracy can satisfy the engineering application requirements. Additionally, it verifies the accuracy and reliability of the indoor anti-skid prediction Equation (10). Given that the equation is obtained through fitting, it requires additional data to verify its generalizability and applicability.

Table 11. Comparison of predicted value and measured value.

Anti-Skid Surface Type		Measured SFC	Equation (10)	Forecast Bias	Deviation Rate
			Forecast SFC		
GAC-16	Option One	57.7	60.5	+2.8	4.6
	Option Two	54.5	64.4	+9.9	15.4
	Option Three	54.2	60.7	+6.6	10.8
	Option Four	53.6	62.7	+9.1	14.6
HET-10		55.3	57.1	+1.8	3.2

Table 12. Comparison of the prediction results of the two equations.

Anti-Skid Surface Type		Equation (11)	Equation (10)	SFX Deviation	Deviation Rate
		Forecast SFC	Forecast SFC		
GAC-16	Option One	57	60.5	+3.5	5.8
	Option Two	52.2	64.4	+12.2	18.9
	Option Three	53	60.7	+7.8	12.8
	Option Four	53.2	62.7	+9.5	15.1
HET-10		55	57.1	+2.1	3.7

In the past few years, several researchers have conducted investigations into anti-skid resistance. For instance, Bernhard Hofko [20] developed a prediction model for skid and polishing resistance that correlated laboratory-based polishing simulation with skid resistance measurement and evaluated the evolution of skid resistance under traffic in the field. Maria Pomoni [25] explored the skid resistance performance of asphalt mixtures containing recycled materials through their polishing behavior under traffic. The study

developed preliminary equations that adequately described the polishing curves of the investigated mixtures, with results demonstrating that the friction level of the tested asphalt mixtures containing RAP or CR is slightly lower than the conventional ones (using the attenuation rate B value to evaluate the anti-skid durability). The accuracy and reliability of the indoor anti-skid prediction equation have been established. Future research should integrate the actual traffic situation and the change rule for asphalt mixture anti-skid resistance into actual engineering to improve the equation using more data.

3.3.3. Evaluation Standard

To ensure safe driving conditions, the “Specification for Design of Highway Asphalt Pavement” (JTGD50-2017) in China mandates that the lateral force coefficient (SFC) of highway asphalt pavement should not fall below 54 (average annual rainfall > 1000 mm). However, the code does not specify the evaluation criteria or standards for the anti-skid durability of asphalt mixtures, despite imposing initial performance requirements. This research identifies the mechanical properties of coarse aggregates, the grading of mineral aggregates, and the cumulative number of truck axle loads (CNAT) as the primary factors affecting the anti-skid durability of asphalt pavement. From the obtained anti-skid attenuation prediction Equation (10), it is evident that the attenuation rate B value determines the anti-skid durability of the asphalt mixture, given that the initial anti-skid performance value is determined. Therefore, to facilitate the evaluation of anti-skid durability during asphalt mixture design, the attenuation rate B value is proposed as an evaluation index. Considering the initial value of the asphalt mixture pendulum value, the cumulative truck axle number, and the highway asphalt pavement maintenance standard (SFC should not be less than 40), the calculated attenuation rate B value should not exceed the value in Table 13 according to Equations (5) and (10). This value ensures that the anti-skid durability of the asphalt mixture meets the corresponding traffic level requirements.

Table 13. Control standard of attenuation rate B value.

CNAT (Million Times)	200	400	800	2000	3000	4000
B value	7.0	6.0	5.1	4.3	4.1	3.9

4. Conclusions

This study employed an indoor small-scale accelerated loading test to investigate the anti-skid performance of asphalt mixtures under water bath conditions. Specifically, six groups of AC-16 and six groups of SMA were tested to evaluate the impact of aggregate lithology, gradation, and asphalt dosage on anti-skid performance. The study proposed an index to evaluate the anti-skid durability of the asphalt mixture. The main findings are summarized below.

- (1) The initial values of the mean texture depth (MTD) and British pendulum number (BPN) of an asphalt mixture are significantly influenced by the gradation and oil-stone ratio. As the oil-stone ratio increases or the gradation becomes finer, the initial MTD value of both AC-16 and SMA-13 gradually decreases. This can be attributed to the presence of asphalt film, which limits the aggregate texture’s anti-skid effect in the initial stage (bitumen masking effect). Furthermore, finer gradation is more likely to result in a higher initial friction coefficient.
- (2) Through an accelerated loading test, the evolution of the mean texture depth (MTD) of AC-16 and SMA-13 under water bath conditions is investigated. The MTD of AC-16 decays rapidly at first, then gradually wears down and finally reaches a stable state as the number of loading cycles increases. However, the MTD of SMA-13 exhibits a wavering trend. Analysis reveals that this phenomenon is mainly due to the slight compaction of the asphalt mixtures during the initial stage of loading, which results in a decreasing trend in the structural depth. With increasing loading cycles, the AC-16 mix enters the phase of angular surface wear, leading to a gradual decay of

- MTD. Conversely, the SMA mix enters the surface asphalt mortar shedding stage, resulting in an increasing trend in its MTD. These findings provide insights into the wear behavior of asphalt mixtures under accelerated loading conditions, highlighting the role of water and tires in the evolution of the surface texture of asphalt mixtures.
- (3) The behavior of two asphalt mixture types, AC-16 and SMA, was investigated under accelerated loading conditions. Specifically, the evolution of the British Pendulum Number (BPN) as the loading frequency increased was analyzed. Results indicate that the BPN of AC-16 displays a biphasic decay trend, characterized by a rapid initial decay (before 20,000 cycles), a stable decay stage (20,000–400,000 cycles), and a relatively stable state thereafter. Conversely, the BPN of SMA show an initial increasing trend followed by a gradual decrease. The thickness of the asphalt film is thought to be responsible for this trend, as it initially prevents the texture from fully exerting its anti-skid effect. The combined action of the loading wheel and water causes the asphalt film to fall off, resulting in an increase in BPN.
 - (4) This study has conducted 600,000 accelerated loading tests to investigate the impact of aggregate lithology, asphalt mixture type, and oil-stone ratio on the anti-skid durability of asphalt pavements. It has been observed that the BPN of the asphalt mixture is influenced by the aggregate's polishing value, crushing value, and abrasion value, with a larger BPN associated with a larger polishing value and smaller crushing and abrasion values. Moreover, the anti-skid index attenuation rate is lower for coarser and finer gradations. The SMA asphalt mixture shows better anti-skid performance and durability than the AC asphalt mixture.
 - (5) A predictive equation for the attenuation of the anti-skid performance of asphalt mixtures was developed and verified. The results of the verification test demonstrated the proposed equation's high accuracy and reliability. The attenuation rate B value was recommended to evaluate the anti-skid durability of the asphalt mixture, with accompanying control standards also presented.

This study has some limitations, as it only conducted an indoor loading experiment. The changes in the anti-skid performance of the asphalt mixture observed in the laboratory may differ from those on actual roads, thus only presenting some general patterns. To address this, further analysis of the anti-skid performance of materials on real roads is necessary, along with improving and verifying the accuracy of the equation based on the usage of asphalt mixture in various projects.

Author Contributions: Research papers and designs: H.W., J.Y., X.X., S.L. and W.H.; data collection: H.W. and X.S.; result analysis and interpretation: Y.L., J.Y. and X.X.; draft preparation: H.W., Y.L. and X.S. All authors have read and agreed to the published version of the manuscript.

Funding: This research was financially supported by the National Key R & D Program of China (Grant No. 2021YFB2601200), the National Natural Science Foundation of China (No. 51778140, No. 52078130), the Major Technology Demonstration of Epoxy Asphalt in Pavement as a Green Highly Efficient Carbon Mitigation Technology of Jiangsu, China (Major Technology Demonstration Program) (No. BE2022615), the Major Science and Technology Project of Nanjing (No. 202209012), and the Technology Research and Development Program of China State Railway Group Co., Ltd. (Beijing 10000, China) (P2019G030).

Institutional Review Board Statement: Not applicable.

Informed Consent Statement: Not applicable.

Data Availability Statement: Data available on request.

Conflicts of Interest: The authors declare no conflict of interest.

References

1. Plati, C.; Pomoni, M.; Stergiou, T. From Mean Texture Depth to Mean Profile Depth: Exploring possibilities. In Proceedings of the 7th International Conference on Bituminous Mixtures and Pavements (ICONFBMP), Thessaloniki, Greece, 12–14 June 2019; pp. 639–644. [\[CrossRef\]](#)
2. Zheng, N.; Bi, J.; Dong, S.; Lei, J.; He, Y.; Cui, Z.; Chen, L. Testing and evaluation for long-term skid resistance of asphalt pavement composite seal using texture characteristics. *Constr. Build. Mater.* **2022**, *356*, 129241. [\[CrossRef\]](#)
3. Yu, M.; You, Z.; Wu, G.; Kong, L.; Liu, C.; Gao, J. Measurement and modeling of skid resistance of asphalt pavement: A review. *Constr. Build. Mater.* **2020**, *260*, 119878. [\[CrossRef\]](#)
4. Yu, Y.; Tang, S.; Xu, G.; Fan, Y.; Wu, Y.; Wang, H.; Yang, J. Investigations on the long-term skid resistance of epoxy asphalt mixture based on accelerated loading test. *Constr. Build. Mater.* **2023**, *365*, 130150. [\[CrossRef\]](#)
5. Zhu, S.; Ji, X.; Zhang, Z.; Shao, D.; Li, H.; Yun, C. Evolution characteristics of the surface texture of the wearing course on asphalt pavement based on accelerated pavement polishing. *Constr. Build. Mater.* **2022**, *333*, 127266. [\[CrossRef\]](#)
6. Wu, X.; Zheng, N.; Lei, J. Study on the changes of texture characteristic parameters of bauxite clinker re placement asphalt mixtures under accelerated loading. *Constr. Build. Mater.* **2021**, *288*, 123160. [\[CrossRef\]](#)
7. Wu, X.; Zheng, N.; Lei, J. Influencing factors and mechanism for the attenuation of the skid resistance for bauxite clinker-asphalt mixtures. *Constr. Build. Mater.* **2021**, *283*, 122670. [\[CrossRef\]](#)
8. Kogbara, R.B.; Masad, E.A.; Kassem, E.; Scarpas, A.; Anupam, K. A state-of-the-art review of parameters influencing measurement and modeling of skid resistance of asphalt pavements. *Constr. Build. Mater.* **2016**, *114*, 602–617. [\[CrossRef\]](#)
9. Xu, X.; Yu, Y.; Yang, J.; Wu, C. Long-Term Skid Resistance Evaluation of GAC-16 Based on Accelerated Pavement Testing. *Adv. Mater. Sci. Eng.* **2020**, *2020*, 1245060. [\[CrossRef\]](#)
10. Lin, C.; Tongjing, W. Effect of fine aggregate angularity on skid-resistance of asphalt pavement using accelerated pavement testing. *Constr. Build. Mater.* **2018**, *168*, 41–46. [\[CrossRef\]](#)
11. Li, J.; Zhu, L.; Yu, M.; Zuo, S.; Cui, X.; Liu, P. Long-Term Performance of Recycled Asphalt Pavement with Recycled Engine Oil Bottom Based on Accelerated Loading Test. *Coatings* **2022**, *12*, 522. [\[CrossRef\]](#)
12. Wu, X.; Chen, Q.; Li, Y.; Dong, N.; Yu, H. Investigating the Deterioration of Pavement Skid Resistance Using an Accelerated Pavement Test. *Materials* **2023**, *16*, 422. [\[CrossRef\]](#)
13. Qian, Z.-D.; Liu, Y.; Liu, C.-B.; Zheng, D. Design and skid resistance evaluation of skeleton-dense epoxy asphalt mixture for steel bridge deck pavement. *Constr. Build. Mater.* **2016**, *114*, 851–863. [\[CrossRef\]](#)
14. Li, J.; Yu, J.; Wu, S.; Xie, J. The Mechanical Resistance of Asphalt Mixture with Steel Slag to Deformation and Skid Degradation Based on Laboratory Accelerated Heavy Loading Test. *Materials* **2022**, *15*, 911. [\[CrossRef\]](#)
15. Azari, H.; Mohseni, A.; Gibson, N. Verification of Rutting Predictions from Mechanistic-Empirical Pavement Design Guide by Use of Accelerated Loading Facility Data. *Transp. Res. Rec.* **2008**, *2057*, 157–167. [\[CrossRef\]](#)
16. Chen, W. Evaluation of Skid-Resistance Decay Characteristic of Asphalt Mixture Based on Pressure-Sensitive Film Technology. In Proceedings of the 2020 International Conference on Artificial Intelligence and Electromechanical Automation (AIEA 2020), Tianjin, China, 26–28 June 2020. [\[CrossRef\]](#)
17. Rezaei, A.; Masad, E. Experimental-based model for predicting the skid resistance of asphalt pavements. *Int. J. Pavement Eng.* **2013**, *14*, 24–35. [\[CrossRef\]](#)
18. Wang, D.; Wang, G. Designing a Skid-Resistant and Durable Asphalt Mixture Based on the Stress Concentration Distribution Rate. *Arab. J. Sci. Eng.* **2017**, *42*, 4131–4144. [\[CrossRef\]](#)
19. Liu, Y.; Cheng, X.; Yang, Z. Effect of Mixture Design Parameters of Stone Mastic Asphalt Pavement on Its Skid Resistance. *Appl. Sci.* **2019**, *9*, 5171. [\[CrossRef\]](#)
20. Hofko, B.; Kugler, H.; Chankov, G.; Spielhofer, R. A laboratory procedure for predicting skid and polishing resistance of road surfaces. *Int. J. Pavement Eng.* **2019**, *20*, 439–447. [\[CrossRef\]](#)
21. Ferkov, S.A.; Soudani, K.; Haddadi, S. Laboratory study of the skid resistance of asphalt concrete made of local low performances aggregates by partially replacing sand with olive mill waste. *Constr. Build. Mater.* **2022**, *324*, 126657. [\[CrossRef\]](#)
22. Villani, M.; Scarpas, A.; de Bondt, A.; Khedoe, R.; Artamendi, I. Application of fractal analysis for measuring the effects of rubber polishing on the friction of asphalt concrete mixtures. *Wear* **2014**, *320*, 179–188. [\[CrossRef\]](#)
23. Xiong, R.; Zong, Y.; Lv, H.; Sheng, Y.; Guan, B.; Niu, D.; Wang, H. Investigation on anti-skid performance of asphalt mixture composed of calcined bauxite and limestone aggregate. *Constr. Build. Mater.* **2021**, *306*, 124932. [\[CrossRef\]](#)
24. Tang, T.; Anupam, K.; Kasbergen, C.; Kogbara, R.; Scarpas, A.; Masad, E. Finite Element Studies of Skid Resistance under Hot Weather Condition. *Transp. Res. Rec. J. Transp. Res. Board* **2018**, *2672*, 382–394. [\[CrossRef\]](#)
25. Pomoni, M.; Plati, C.; Kane, M.; Loizos, A. Polishing behaviour of asphalt surface course containing recycled materials. *Int. J. Transp. Sci. Technol.* **2022**, *11*, 711–725. [\[CrossRef\]](#)

Disclaimer/Publisher's Note: The statements, opinions and data contained in all publications are solely those of the individual author(s) and contributor(s) and not of MDPI and/or the editor(s). MDPI and/or the editor(s) disclaim responsibility for any injury to people or property resulting from any ideas, methods, instructions or products referred to in the content.